AIAA SciTech Forum
4-8 January 2016, San Diego, California, USA
54th AIAA Aerospace Sciences Meeting

10.2514/6.2016-0507

Limits for Thermionic Emission from Leading Edges of Hypersonic Vehicles

Kyle M. Hanquist* and Iain D. Boyd†
Department of Aerospace Engineering, University of Michigan, Ann Arbor, MI

Abstract

Simulations of electron transpiration cooling (ETC) on the leading edge of a hypersonic vehicle using computational fluid dynamics (CFD) are presented. The thermionic emission boundary condition and electric field model including forced diffusion are discussed. Different analytical models are used to describe the plasma sheath physics in order to avoid resolving the sheath in the computational domain. The first analytical model does not account for emission in the sheath model, so the emission is only limited by the surface temperature. The second approach models the emissive surface as electronically floated, which greatly limits the emission. The last analytical approach biases the emissive surface, which makes it possible to overcome space-charge limits. Each approach is compared and a parametric study is performed to understand the effects that the material work function, freestream velocity, and leading edge geometry has on the ETC effect. The numerical results reveal that modeling the sheath as a floated surface results in the emission, and thus ETC benefits, being greatly limited. However, if the surface is negatively biased, the results show that the emission can overcome space-charge limits and achieve the ideal ETC benefits predicted by temperature limited emission. The study also shows that, along with negatively biasing the surface, emission is enhanced by increasing the number of electrons in the external flowfield by increasing the freestream velocity.

Nomenclature

A_R	Richardson constant, 1.20×10^6 A/m^2/K^2
C_s	Charge of species s
$\bar{C}$	Thermal speed
D	Diffusion coefficient
$\mathbf{E}$	Electric field
$\mathbf{j}$	Electric current density
$\mathbf{J}$	Diffusive flux
J	Current density
$\hbar$	Planck constant, 6.63×10^{-34} m^2 kg/s
k_B	Boltzmann constant, 1.38×10^{-23} J/K
K	Mobility
m_s	Mass of species s
M_s	Molar mass of species s
n	Number density
N_{Av}	Avogadro constant, 6.02×10^{23} mol^{-1}
p	Pressure
q	Heat transfer
Q_e	Elementary charge, 1.60×10^{-19} C
u	Velocity
$\mathbf{U}$	Drift velocity

*PhD Candidate, Student Member AIAA.
†James E. Knott Professor of Engineering, Fellow AIAA

R_n Leading edge radius
R_u Universal gas constant
s Distance along leading edge
T Temperature
$\dot{w}_s$ Production rate of species s
Y Mass fraction
α Polarizability
Γ Ratio of emission to flowfield electron current densities
ϵ_0 Vacuum permittivity, 8.85×10^{-12} F/m
λ_D Debye length
λ_{mfp} Mean free path
μ Reduced mass
ν Collisionality
ϕ Electric potential
Φ Material work function
ρ Density
σ Electrical conductivity
σ_{s-s} Collisional cross-section area
ψ Normalized sheath voltage

Subscript
e Electron
e Emitted
i Ion
f Flowfield
tr Translational
vib Vibrational
w Wall
∞ Freestream

I. Introduction

One of the most limiting factors in hypersonic vehicle development is the need for effective thermal management of the large heat fluxes experienced during flight. By definition, a hypersonic vehicle travels at high velocities and in order to maintain these speeds the vehicle is designed to have a sharp leading edge to increase the lift-to-drag ratio. However, the aerodynamic performance gains obtained by having a sharp leading edge come at the cost of very high, localized heating rates. A theoretical analysis first performed by Fay and Riddell[1] shows that the stagnation point heating is proportional to the freestream velocity cubed and inversely proportional to the leading edge radius,

$$q_w \propto \sqrt{\frac{\rho_\infty}{R_n}} u_\infty^3 \tag{1}$$

Equation 1 reveals that two of the main characteristics of hypersonic flight, high velocity and sharp leading edges, lead to massive heat transfer to the vehicle. One approach to address this issue is to use a leading edge material that can withstand the high heating rates and temperatures. An ideal material would have good thermal properties (able to withstand high temperatures while being minimally conductive) and also be lightweight, because the thickness of the material will be limited by the leading edge radius and its weight. One type of material that has good thermal properties is ultra-high temperature composite (UHTC) materials, which were used on the NASA X-43 experimental hypersonic aircraft.[2] Although UHTC materials have good thermal properties, they have some physical limitations such as heavy weight and weak fracture toughness that suggest they are not the ideal approach.[3] Another approach to manage the heat loads is to reject the heat passively, either through heat-shield ablation or radiation. Ablation has significant heat management benefits through essentially a controlled melt of the heat shield while also being light-weight, which makes it a great approach for re-entry flight. This shape change of the surface, while permitted for the blunt bodies of re-entry flight, is unacceptable for the sharp leading edges of hypersonic vehicles. Heat management through radiation does not incur shape change, but is limited by the Stefan-Boltzmann law.

An alternative approach that has been proposed recently involves using thermo-electric materials at the leading edges of hypersonic vehicles.[4] When exposed to high convective heating rates, these materials emit a current of electrons that may lead to a transpiration cooling effect of the surface of the vehicle. This phenomenon is known as thermionic emission and occurs when the thermal energy given to the electrons is greater than the binding potential of the surface material. A recent conceptual study was completed and showed thermionic emission can reduce the surface temperature by approximately 40% for a Mach 19.4 flow over a sharp leading radius at an altitude of 60 km with a material work function of 2.0 eV.[5] The essential idea behind electron transpiration cooling (ETC) is that the electrons will carry energy away from the surface, which complements the radiative energy from the surface and balances with the convective energy to the surface. Given the promising trends in that study, further research is needed to improve the modeling capabilities. The modeling approach for ETC was recently compared against a set of experiments and agreed well.[6] This paper focuses on the plasma physics occurring near the emissive surface. A plasma sheath will form near the vehicle surface, which is a region of non-neutral potential. This region will affect and possibly limit the amount of emission from the leading edges of hypersonic vehicles. This study aims to assess the effect plasma sheath physics has on electron transpiration cooling. First, a description of the numerical method and test case conditions are outlined. Then, numerical results are presented that highlight the differences between the emission limits through a parametric study. The parametric study investigates the effect of material work function, freestream velocity, and leading edge geometry has on emission limits and ETC. Finally, the paper presents some conclusions drawn from this study and outlines future work recommendations.

II. Numerical Approach

The numerical simulations in this work are performed using the CFD code LeMANS, which was developed at the University of Michigan.[7] LeMANS is a parallel, three-dimensional code that solves the laminar Navier-Stokes equations on unstructured computational grids. LeMANS includes thermo-chemical non-equilibrium effects and the flow is modeled assuming that the continuum approximation is valid. It is also assumed that the translational and rotational energy modes can be described by a single temperature, T_{tr}, and that the vibrational, electronic, and electron translational energy modes are described by a different temperature, T_{vib}. The mixture transport properties are calculated using Wilke's semi-empirical mixing rule,[8] species thermal conductivities determined using Eucken's relation,[9] and species viscosities determined using Blottner's curve fits.[10] A standard finite-rate chemistry model is used for eleven species reactive air (N_2, O_2, NO, N, O, N_2^+, O_2^+, NO^+, N^+, O^+, and e^-), and Park's two-temperature model[11] is used to account for the effects of thermal nonequilibrium on the forward and backward reactions rates.

In LeMANS, the set of governing equations are solved using the finite-volume method applied to unstructured grids with second order spatial accuracy. A modified Steger-Warming Flux Vector Splitting scheme[12] is used to discretize the inviscid fluxes across cell faces. The viscous terms are computed using cell-centered and nodal values. The viscous stresses are modeled assuming the flow is a Newtonian fluid and Stokes' hypothesis is applicable, and the heat fluxes are modeled according to Fourier's law for all temperatures. For parallel execution of LeMANS, METIS[13] is used to partition the computational mesh, and the Message Passing Interface (MPI) is used to communicate the necessary information between processors.

A. Electron Emission

A boundary condition is implemented into LeMANS to model thermionic emission at the material surface. The production rate of electrons is calculated by,

$$\dot{w}_e = \frac{J_{e,\mathbf{e}}}{Q_e N_{Av}} - \sum_{s=ions} \dot{w}_s \tag{2}$$

where $J_{e,\mathbf{e}}$ is the emission current density, Q_e is the elementary charge, N_{Av} is the Avogadro constant, and $\dot{w}_i$ is the recombination rate of ions. The ions at the surface combine with the emitted electrons to form corresponding neutrals. The current density is calculated using Richardson's Law:[14]

$$J_{e,\mathbf{e}} = A_R T_w^2 exp\Big(\frac{-\Phi\ Q_e}{k_B T_w}\Big) \tag{3}$$

where A_R is a material-constant assumed to be equal to 1.20×10^6 A/m^2/K^2 in the current work, T_w is the surface temperature, k_B is the Boltzmann constant, and Φ is the material work function defined as the minimum energy required to remove an electron from the material. In the current work, the work function varies between 2.0 eV (similar to cesium[15]) and 2.4 eV. It is to be noted that in the current work, electrons can only be emitted from the surface using Richardson's law and are assumed not to recombine back to the surface via Richardson's law. The recombination rate of ions is calculated assuming that the surface is fully catalytic to ions:[16]

$$\dot{w}_i = \frac{\rho_i}{M_i}\sqrt{\frac{R_u T_w}{2\pi M_i}} \tag{4}$$

where ρ_i is the ion density, m_i is the ion mass, and R_u is the universal gas constant. The emitted electrons will carry away energy from the vehicle surface at a flux of:

$$q_{emiss} = J_{e,\mathbf{e}}\Big(\Phi + \frac{2k_B T_w}{Q_e}\Big) \tag{5}$$

B. Electric Field

The electric field can be replaced by an electric potential, ϕ, as,

$$\vec{E} = - \bigtriangledown \phi \tag{6}$$

where the electric potential is calculated using Ohm's law and solving the steady state current continuity equation,

$$\vec{j} = \sigma \vec{E} \tag{7}$$

$$\bigtriangledown \cdot \vec{j} = \bigtriangledown \cdot (\sigma \bigtriangledown \phi) = 0 \tag{8}$$

where σ is the electrical conductivity of the plasma. The electrical conductivity in this work is approximated using a semi-empirical model developed by Razier,[17] which is valid for air, nitrogen, and argon,

$$\sigma = 8300 \times exp\Big(\frac{-36,000}{T}\Big) \tag{9}$$

A zero-gradient condition is used at the inlet, outlet, and symmetry computational boundaries for the electric potential. At the wall, the electric potential is driven by the plasma sheath physics discussed in Section C. The diffusive fluxes for charged species (ions and electrons) are modified to account for the drift velocity induced by the electric field (forced diffusion),

$$\vec{J_s} = -\rho D_s \bigtriangledown Y_s + \vec{J}_{fd,s} + \vec{J}_s^{SM} \tag{10}$$

where ρ is the density, D_s is the diffusion coefficient of species s, and Y_s is the mass fraction. The $\vec{J}_s^{SM}$ term appears due to Stefan-Maxwell treatment to ensure mass conservation.[18] For ions, the forced diffusion contribution ($\vec{J}_{fd}$) is,

$$\vec{J}_{fd,i} = \rho \vec{U}_{d,s} Y_i C_i \tag{11}$$

where C_i is the charge number (1 for ions) and $\vec{U}_d$ is the drift velocity. The drift velocity can be calculated in terms of the ion drift-diffusion approximation,[19]

$$\vec{U}_{d,s} = \big(C_s K_s - \sum_j C_j K_j Y_j\big)\vec{E} \tag{12}$$

where K_s is the ion mobility of species s and $\vec{E}$ is the electric field. The ion mobility can be approximated by the polarization limit model[20] and Blanc's law,

$$K_{s,j} = \frac{13.853 \cdot 10^{-4}}{\sqrt{\alpha_{p,j}\mu}} \tag{13}$$

$$\frac{1}{K_s} = \sum_j \frac{Y_j}{K_{s,j}} \tag{14}$$

where $\alpha_{p,j}$ is the polarizability[21] of species j and μ is the reduced mass of species s and j. This is only an approximation because the model assumes the ion mobility is independent of temperature whereas experiments show positive temperature dependence for air ions.[22] For electrons, the forced diffusion contribution is,

$$\vec{J}_{fd,e} = K_e \rho Y_e \vec{E} \tag{15}$$

where the electron mobility can be approximated by the Einstein Relation:

$$K_e = \frac{Q_e D_e}{k_B T_e} \tag{16}$$

where T_e is the electron temperature (assumed to be the same as vibrational temperature in this study). The electric field at the wall can decrease the energy barrier that the emitted electrons must overcome at the surface, which effectively reduces the work function, known as the Schottky effect:[23]

$$\Phi_c = \Phi - \sqrt{\frac{Q_e^3 E_w}{4\pi\epsilon_0}} \tag{17}$$

where E_w is the electric field at the wall and ϵ_0 is the vacuum permittivity. Previous work showed that the magnitude of the electric field for cases similar to this study has a relatively small magnitude, which causes negligible effects on the predicted surface properties of hypersonic vehicles with thermo-electric TPS materials.[5]

C. Plasma Sheath

A plasma or debye sheath forms near the the wall, which is a non-neutral region between the quasineutral flowfield and the wall. The sheath occurs because the electrons are much more mobile than the ions due to their mass ($m_e \ll m_i$) and temperature ($T_e \geq T_i$) difference. This higher mobility of electrons leads to more electrons leaving this region than ions, leaving the region positively charged, which generates a potential difference between the flowfield and the wall. The length scale of this non-neutral region is on the order of the Debye length:

$$\lambda_D = \sqrt{\frac{\epsilon_0 k_B T_e}{Q_e^2 n_e}} \tag{18}$$

Another important sheath parameter is the sheath collisionality, which is proportional to the number of collisions that occur within the sheath,

$$\nu \equiv \frac{\lambda_D}{\lambda_{mfp}} \tag{19}$$

where λ_{mfp} is the mean free path. The mean free paths of interest are the ion-neutral and electron-neutral mean free paths:

$$\lambda_{mfp,i-n} = \frac{1}{(n_i + n_{neut})\sigma_i}, \quad \lambda_{mfp,e-n} = \frac{1}{(n_e + n_{neut})\sigma_e} \tag{20}$$

where σ_i and σ_e are the collisional cross sections of the ions and electrons, respectively. For the cases of interest, the Debye length ($\sim \mu m$) is much smaller than the ion-neutral and electron-neutral mean free paths ($\sim mm$), which leads to the collisionality of the sheath being much smaller than one. Since $\nu \ll 1$, the sheath can be treated as collisionless.[24] This is important because it is difficult to resolve the sheath in the computational mesh because it would require many more cells to capture the sheath physics due to its small length scale. An analytical model can be then used to model the sheath physics and the sheath edge will act as the *wall* or *surface* boundary condition in the CFD code.

1. Neglect effect of emission

In previous ETC modeling, the effect of emission on the plasma sheath was neglected. If the emitted electrons are neglected, the wall potential is calculated by assuming the flowfield ion and electron fluxes are equal at the wall,[25,26]

$$\phi_w = \frac{k_B T_e}{Q_e} log\left(\frac{n_i}{n_e}\sqrt{\frac{2\pi m_e(T_i+T_e)}{m_i T_e}}\right) \tag{21}$$

where n_i and n_e are the ion and electron number densities, T_i and T_e are ion and electron temperatures (assumed to be equal to T_w in this work), and m_i and m_e are the ion and electron masses. This case will be referred to as T limited emission, in that the level of emission will only be limited the wall temperature (Eq. 3).

2. Zero net sheath current

If the emission is not neglected, plasma sheath physics will have an effect on emission. If this surface is treated as an electronically floating surface, the net current through the sheath must be zero:

$$J_{e,\mathbf{e}} = J_{i,\mathbf{f}} - J_{e,\mathbf{f}} \tag{22}$$

Essentially, the amount of electrons that *escape* the sheath will be limited by the difference between flowfield ions and electrons reaching the sheath edge. Since the flowfield is quasineutral, the level of emission for treating the wall as an electronically floated surface is small. Since the net charge flow through the sheath edge is zero, the potential boundary condition for the sheath edge will be a zero gradient. The wall potential can be approximated using relations provided by Hobbs and Wesson:[27]

$$\phi_w \approx \frac{-k_B T_e}{Q_e} log\left[\frac{1-\Gamma}{\sqrt{\frac{2\pi m_e}{m_i}}}\right] \tag{23}$$

where Γ is the ratio of the emission (see Eq. 3) to flowfield ($J_{e,\mathbf{f}}$) electron fluxes. This approximation assumes that the ions arrive at the wall cold and the electrons are emitted with negligible energy. The flowfield electron current density can be calculated by,

$$J_{e,\mathbf{f}} = Q_e n_{e,\mathbf{f}} \sqrt{\frac{k_B T_e}{2\pi m_e}} exp\Big(\frac{Q_e \phi_w}{k_b T_e}\Big) \tag{24}$$

where $n_{e,\mathbf{f}}$ is the number density of flowfield electrons, which is assumed to equal the number density of flowfield electrons at the sheath edge without emission (assume emission has no effect on $n_{e,\mathbf{f}}$). This approximation is good up to Γ_{crit} in which a potential well forms such that a fraction of the emitted electrons return to the wall to maintain the current conservation in the sheath region. These critical values are space charge limited values.[27]

$$\Gamma_{crit} = 1 - 8.3\sqrt{\frac{m_e}{m_i}} \tag{25}$$

$$\phi_{w,crit} = \frac{-1.02 k_B T_e}{Q_e} \tag{26}$$

Writing Eq. 22 in terms of Γ:

$$J_{e,\mathbf{e}} = \frac{\Gamma}{1-\Gamma} J_{i,\mathbf{f}} \tag{27}$$

As expected, emission is limited by both flowfield ions and electrons. The lightest ion in air is N^+ and the heaviest is O_2^+ which will lead to Γ_{crit} being between 0.94 and 0.97. This case will be referred to Z-C limited emission, in that the level of emission is limited by a zero net current through the sheath.

3. Net sheath current

If the surface is not floating electrically and is negatively biased, a net current is permissible through the sheath edge. A way this would be possible would be if electrons reattached downstream on the vehicle surface and flowed back to the emissive surface, completing the circuit. An important limit in this regime is space-charge limited emission. Space-charge limited emission occurs when there is a significant electron cloud in front of the emissive surface, which creates a virtual cathode that forces the electrons back to the surface. Ye and Takamura[28] derived an expression for space-charge limited current through the sheath assuming zero electric field condition on the material surface:

$$J_{e,\mathbf{e}} = \frac{G}{2(1+G)} Q_e n_{e,\mathbf{f}} \bar{C}_e \sqrt{-\pi\psi} \tag{28}$$

$$\psi = \frac{Q_e \phi_s}{T_e} \tag{29}$$

$$\bar{C}_e = \sqrt{\frac{8T_e}{\pi m_e}} \tag{30}$$

$$G = f(\psi) \tag{31}$$

where $\bar{C}_e$ is the electron thermal speed, ψ is the normalized sheath voltage of the surface relative to the local plasma, ϕ_s is the sheath voltage drop (difference between wall and sheath edge potential), and $n_{e,\mathbf{f}}$ is the flowfield electron number density at the sheath edge, which is assumed to equal the number density of flowfield electrons at the sheath edge without emission. For Eqs. 29 and 30, the electron temperature is assumed to equal the wall temperature. A schematic of the sheath is shown in Fig. 1. This case will be referred to as *S-C* limited emission, in that the the level of emission is limited by space-charge.

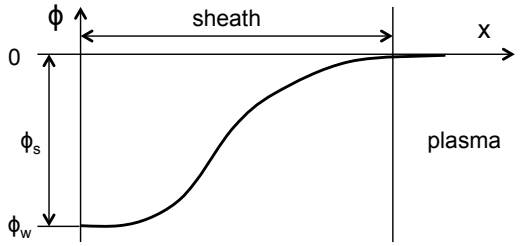

Figure 1: Plasma sheath schematic

III. Test Case Description

The geometry of the test case considered in this study is representative of a 2D leading edge of a hypersonic vehicle and is shown in Fig. 2. The leading edge nose radius is 1.0 cm (unless otherwise stated), the wedge angle is 5.0 deg., and the length of the model is 25 cm. The material radiative emissivity is assumed to equal 1.0. A mesh was generated for the geometry, and a grid convergence study revealed that the solution is grid-independent. Only one-half of the leading edge geometry is considered in the numerical simulations in order to reduce the computational cost using the axial vector as the line of symmetry. The computational grid contains approximately 20,000 cells, with 160 cells normal to the vehicle and 125 cells along the surface. The freestream conditions correspond to conditions at 60 km altitude and are listed in Table 1. The freestream velocity is 6 km/s and material work function is 2.0 eV unless otherwise noted.

Table 1: Freestream properties

Velocity, km/s	Temperature, K	Density, kg/m^3
6	238	2.30×10^{-4}

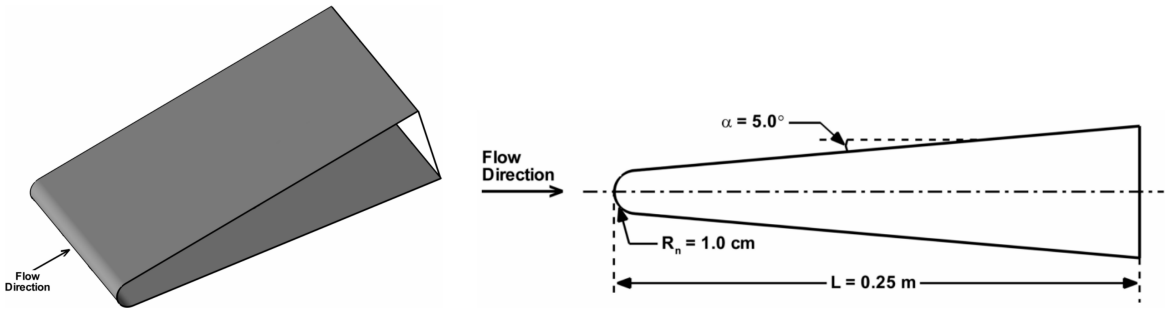

(a) 3-D View (b) Cross-Sectional View

Figure 2: Test case geometry

IV. Numerical Results

The goal of this study is to perform an analysis of the effect that limited electron emission has on electron transpiration cooling of leading edges of hypersonic vehicles that employ thermo-electric TPS materials. In this study, different approaches are taken for modeling the plasma physics near the leading edge. For each approach, a parametric study is carried out to understand the the effects that material work function, freestream velocity, and the leading edge radius has on this cooling effect.

A. Flowfield features

The flowfield features for the conditions typical of those investigated in this study are shown in Figs. 3, which show the temperature contours for the 6 km/s case without ETC and with ETC ($\Phi = 2.0$ eV) and the temperature profiles along the stagnation line. The flow for both cases is characterized by a strong bow shock that develops around the leading edge. The translational temperature rises to over 16,000 K across the shock before decreasing in the shock layer. The figure also shows that ETC has an overall small effect on the flowfield features. However, the shock standoff distance is slightly smaller and the surface temperature is lower for the case with electron emission.

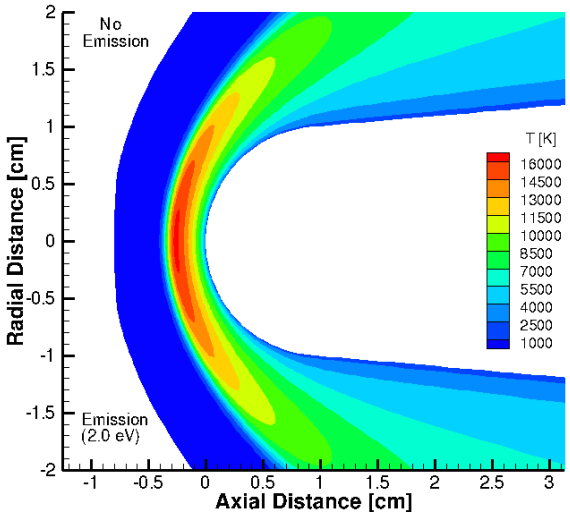

(a) Temperature contours: without emission (top); with emission (bottom)

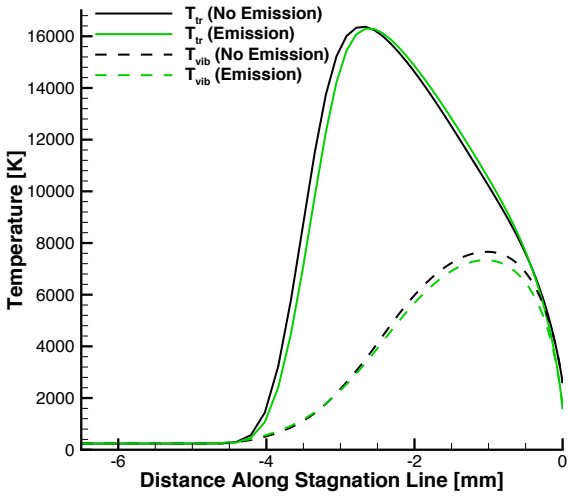

(b) Temperature profiles along stagnation line

Figure 3: Temperature and number density profiles along the stagnation line for the T-limited 6 km/s case

B. Emission limits

In this section, the effects of different analytical sheath models, work function, freestream velocity, and leading edge geometry have on the level of emission and ETC are evaluated.

1. Material work function

For each type of limit; temperature (T), zero sheath current (Z-C), and space-charge (S-C), two different material work functions are considered, 2.0 and 2.4 eV. Figure 4 presents the emission current density for the T and S-C limits for a material work function of 2.0 and 2.4 eV. Note that the distance along the leading edge (s) is normalized by the leading edge radius. The T-limited current density will be the upper limit to the emission because it is only limited by the wall temperature (Eq. 3). The S-C limit can limit the T-limited current due to space-charge limits. Figure 4 shows that emission does not reach this space-charge limit and the emission will not be limited by space-charge for the flowfield and material conditions considered. Figure 5 shows the emission current density (note the change of units) for Z-C limited emission. The emitted current is very limited compared to the T-limited current, which is expected because for Z-C type limits, the net current through the sheath must be zero, and since the flowfield is quasineutral a negligible amount of emission would be expected. The surface temperature and convective heat transfer for each case is presented in Figs. 6 and 7. Figure 6 shows the T-limited surface properties. Similar to what has been shown in previous work, ETC results in a significantly lower surface temperature. Higher level of emissions correspond to decreased surface temperatures. As shown in Fig. 3, emission has a minimal effect on the flowfield temperature so the lower surface temperature results in a higher temperature gradient, which results in higher convective heat transfer for ETC. Since the conditions considered did not reach space-charge limited emission, the S-C surface properties equal the temperature limited surface properties. Figure 7 shows the Z-C limited surface properties. Since the emission for this case is greatly limited, the decrease in surface temperature and corresponding increase in convective heat transfer is much smaller than for the T-limited case. However, it is interesting that such a low level of emission for the Z-C case still results in a noticeable decrease in surface temperature. This is caused by the increase in diffusive heat transfer shown in Fig. 8. Diffusive heat transfer is negligible for the case without emission. For the case with emission, the surface is assumed to be fully-catalytic, which results in an increase in diffusive heat transfer to the wall from the exothermic recombination of emitted electrons to the flowfield ions. The increase in diffusive heat transfer contributes to the convective heat transfer and an increase in convective heat transfer corresponds to a decrease in surface temperature (Fourier's law) given that emission has a negligible effect on the flowfield temperature.

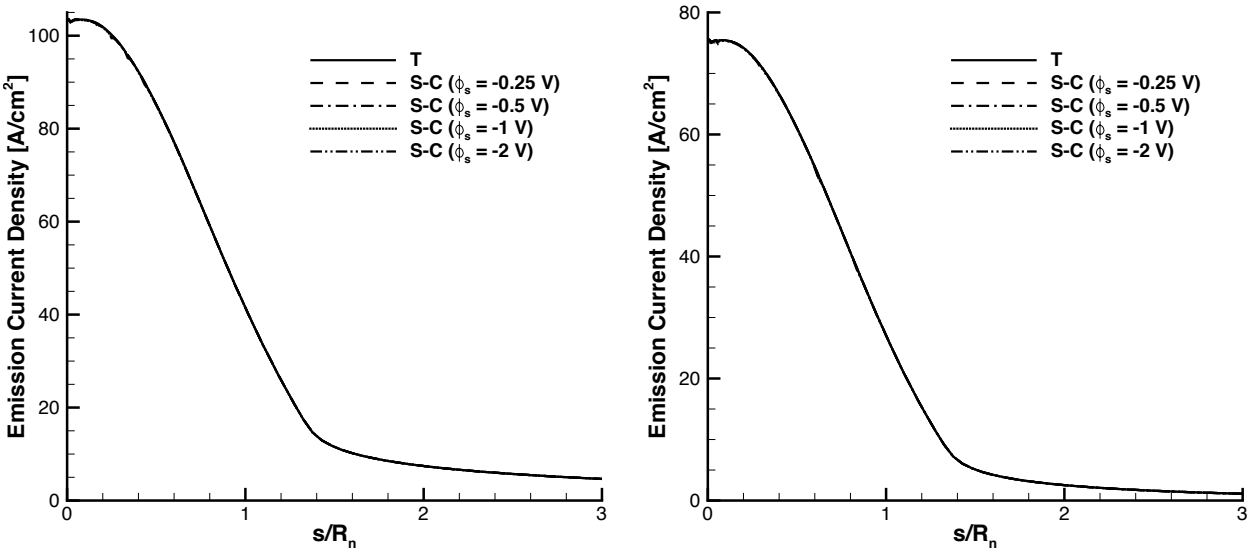

(a) $\Phi = 2.0$ eV (b) $\Phi = 2.4$ eV

Figure 4: Emission current densities for T and S-C limited for different work functions

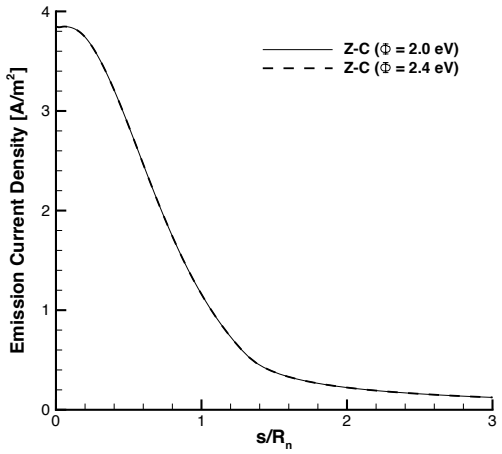

Figure 5: Emission current densities for Z-C limited for different work functions

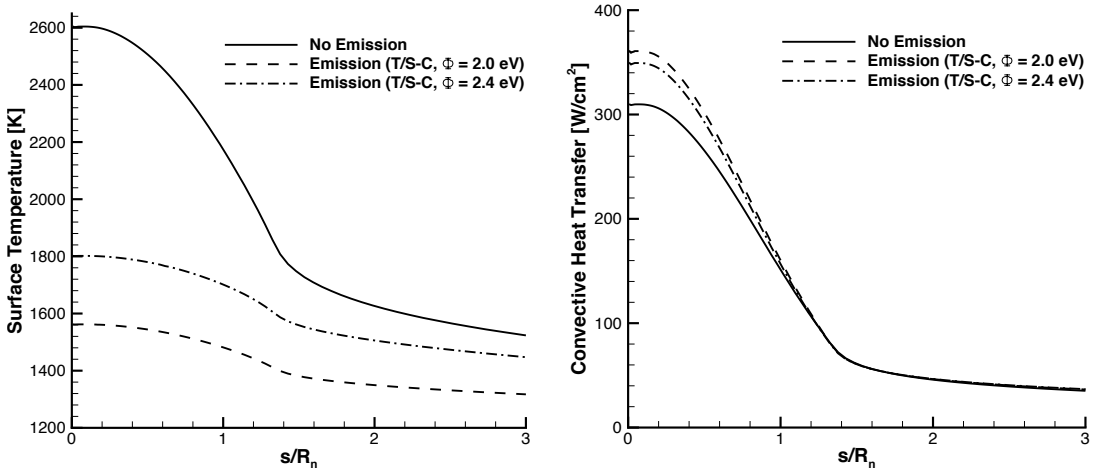

(a) Temperature (b) Heat Transfer

Figure 6: Surface profiles for T limited for different work functions

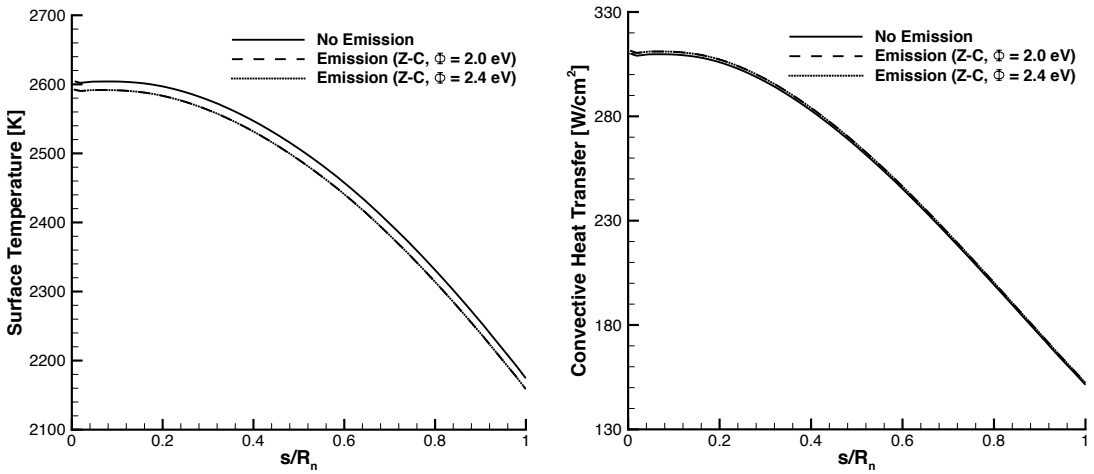

(a) Temperature (b) Heat Transfer

Figure 7: Surface profiles for Z-C limited for different work functions

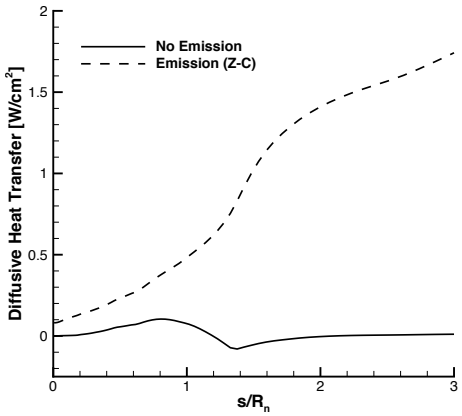

Figure 8: Diffusive heat transfer for Z-C limited

2. *Freestream velocity*

For each type of limit; temperature (T), zero sheath current (Z-C), and space-charge (S-C), two additional freestream velocities are considered in this section, 4 and 8 km/s. Figure 9 shows the emission current densities for temperature and S-C type limits for different velocites. Figure 9a presents the emitted current density for both T and S-C type limits and shows that for a freestream velocity of 4 km/s, the emission becomes space-charge limited for the S-C case for each sheath voltage value considered. As the magnitude of the sheath voltage is increased for the S-C cases, the emission also increases as expected. Since each voltage value is limited, in order to reach the maximum emission (Richardson's current) for the conditions considered, the sheath voltage would have to be more negatively biased than 1 V. Figure 9b shows that emission is not space charge limited for the 8 km/s cases. For the higher velocities (6 and 8 km/s), the emission does not reach the space-charge limit. Although these velocities have high wall temperatures, which have the potential to result in higher emissions due to Eq. 3, the current is not limited due to the large number density of flowfield electrons at the sheath edge as shown in Fig. 10. The higher density of flowfield electrons result from the higher velocity of the vehicle, which results in a stronger shock temperature and more ionization. Essentially with S-C limits, emission is encouraged by having a higher freestream velocity. For the Z-C cases, emission is still greatly limited as shown in Fig. 11. Emission is higher for the higher velocity case (8 km/s). Figure 12 shows the resulting surface temperature and heat transfer for the 4 km/s freestream velocity cases. The resulting surface temperature and convective heat transfer for the S-C and Z-C cases are equal for the 4 km/s cases. Figure 13 presents the surface temperature and heat transfer for the 8 km/s freestream velocity cases. Since the emission is not limited for the S-C cases, the surface temperature and heat transfer are identical to the T-limited profiles.

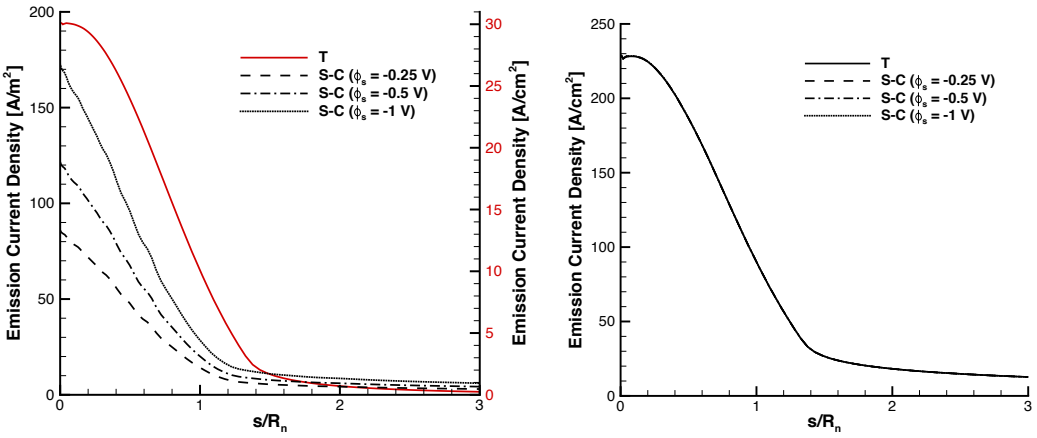

(a) 4 km/s (b) 8 km/s

Figure 9: Emission current densities for T and S-C limited for different freestream velocities

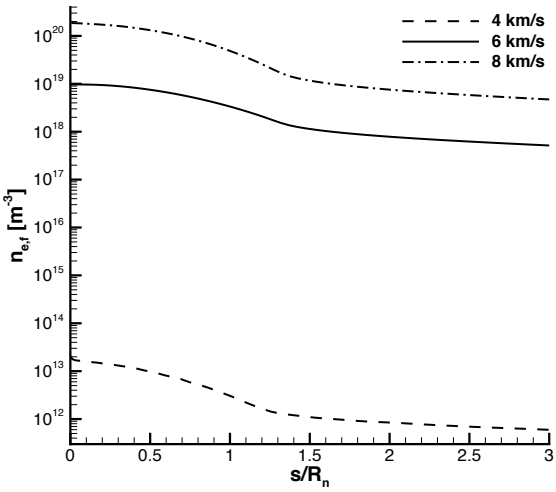

Figure 10: Flowfield electron number density at sheath edge

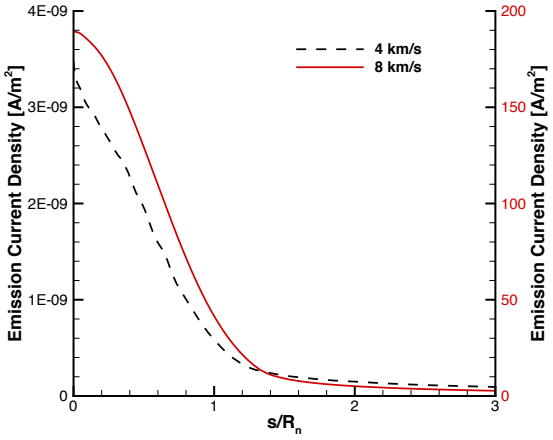

Figure 11: Emission current density for Z-C type limits for different freestream velocities

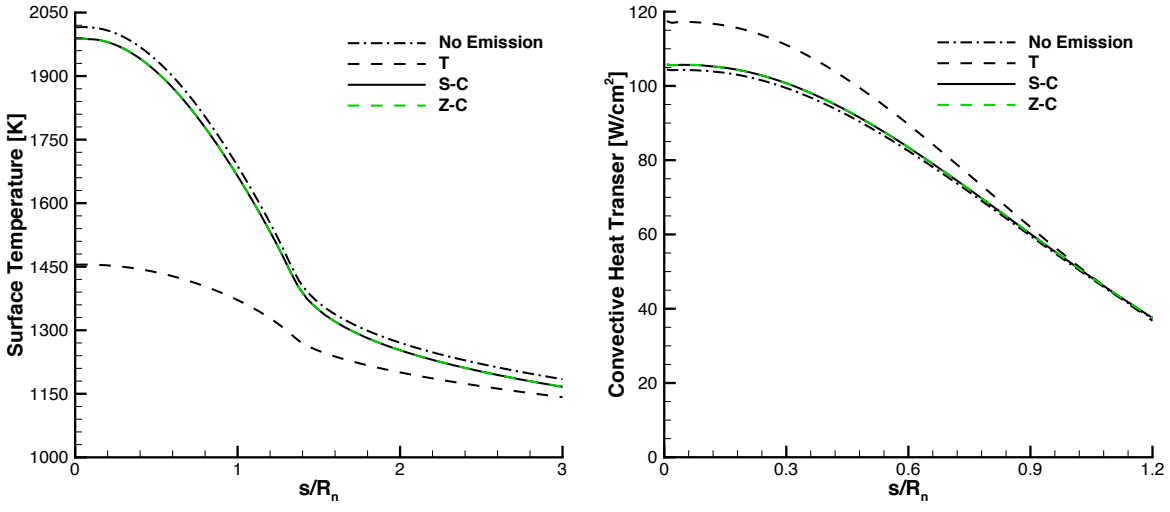

(a) Temperature

(b) Heat Transfer

Figure 12: Surface temperature and heat transfer profiles for 4 km/s freestream velocity

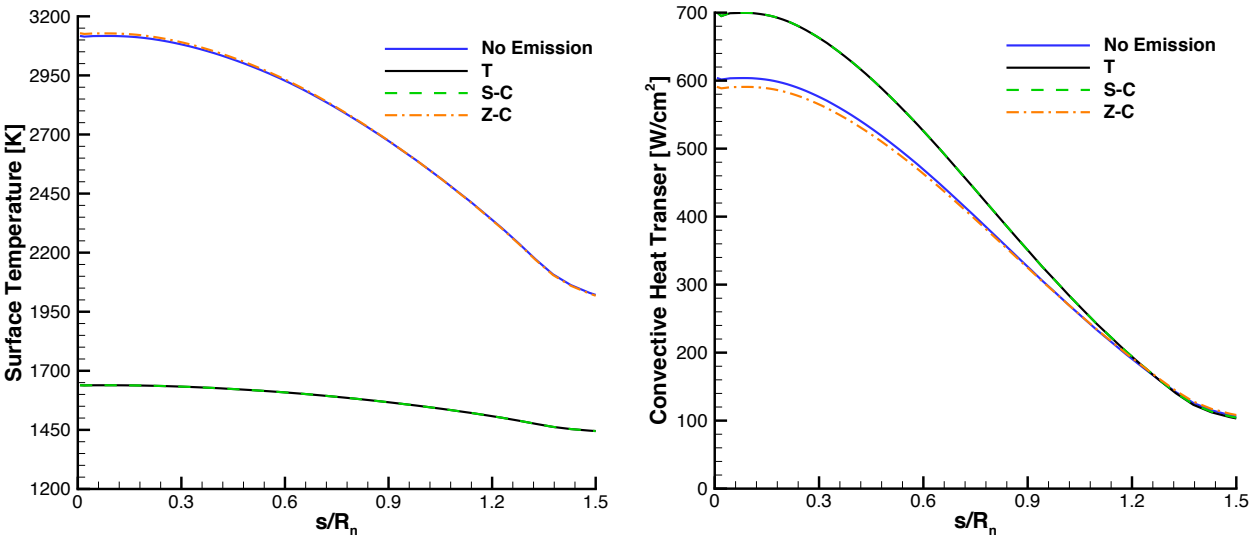

(a) Temperature (b) Heat Transfer

Figure 13: Surface temperature and heat transfer profiles for 8 km/s freestream velocity

3. *Leading edge geometry*

For each type of limit; temperature (T), zero sheath current (Z-C), and space-charge (S-C), an additional leading edge radius at 5.0 cm is considered in this section. Figure 14a presents the emission current density for the T and S-C cases and shows that emission is still not space-charge limited even for a larger leading edge radius. Figure 14b shows the emitted current for the Z-C case is still greatly restricted. All the emission current densities are smaller compared to the smaller leading edge radius cases. The surface profiles for the temperature and heat transfer are presented in Fig. 15. The larger leading edge radius results in lower surface temperatures and convective heat transfer compared to the 1 cm nose radius cases as expected given Eq. 1.

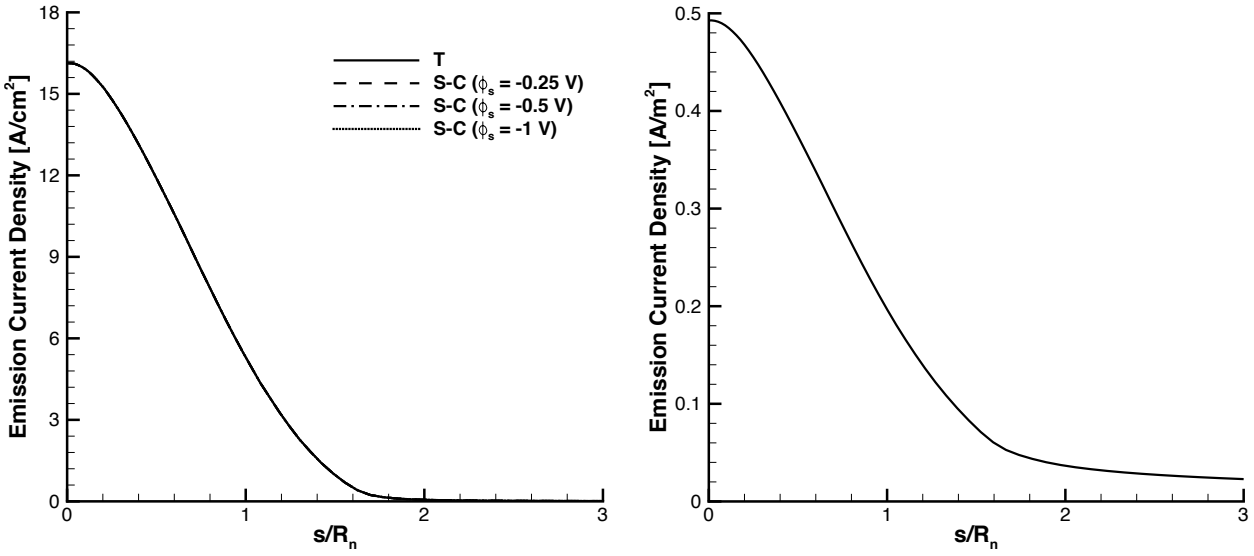

(a) T and S-C limited (b) Z-C limited

Figure 14: Emission current densities for 5 cm leading nose radius

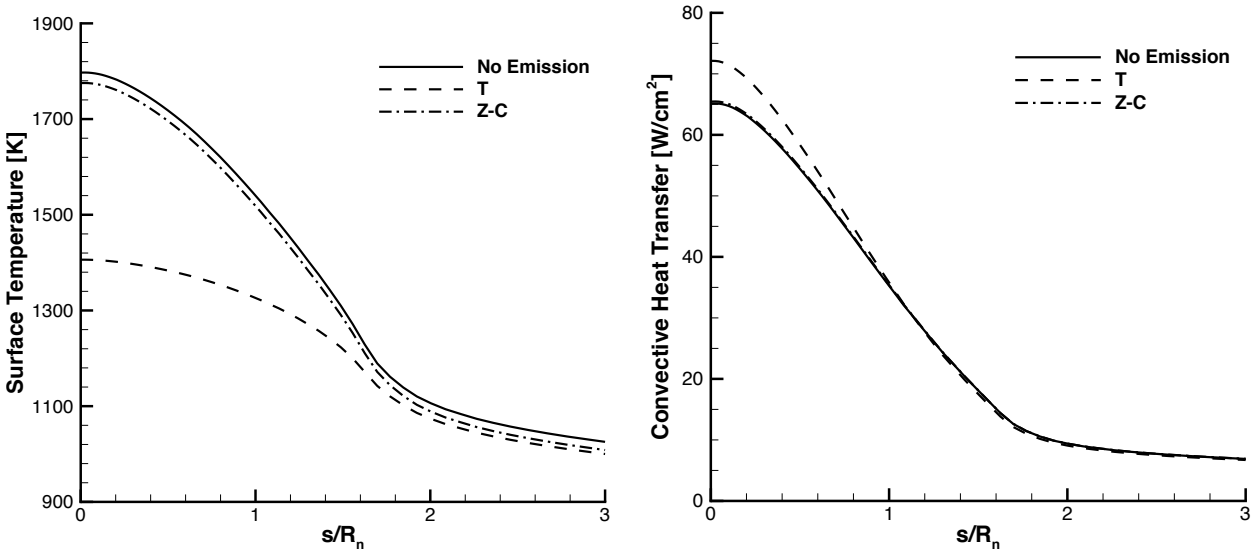

(a) Temperature (b) Heat Transfer

Figure 15: Surface temperature and heat transfer profiles for 5 cm leading nose radius

V. Conclusions and Future Work

The goal of the present work was to assess the effect plasma sheath physics has on electron transpiration cooling (ETC). Three different analytical models were compared. For the first approach, emission was only limited by the surface temperature (T) and the wall potential was modeled neglecting the effect of emission. The second model, Z-C, treated the emissive surface as an electronically floating surface and restricted any net current flow through the sheath. The final model, S-C, introduced a biased sheath voltage that allowed for a net current flow through the sheath, but still could be limited by space-charge build up. The baseline conditions considered in this study were air flow at a freestream velocity of 6 km/s over a 1 cm leading edge radius. The study showed that the Z-C model greatly limited ETC for each case studied. The S-C model with a biased sheath potential often matched the ETC benefits expected for Richardson type emission. This suggests that in order for ETC to be beneficial to hypersonic flight, the emitting surface must have a biased surface potential. The parametric study revealed that having a higher freestream velocity encourages emission for the S-C model, which is promising for hypersonic flight.

In order to continue to improve the modeling capabilities of ETC, future work includes developing an approach that would calculate the minimal amount of sheath voltage, ϕ_s, that would result in temperature limited emission for the S-C cases. The analytical sheath models implemented in LeMANS will be compared against a kinetic 1D sheath code in order to validate the approach.[29] Future work will also investigate the effect of ETC on a full-scale hypersonic vehicle including collecting the emitted electrons downstream on the vehicle to complete the circuit.

Acknowledgements

The authors gratefully acknowledge support for this work from the Lockheed-Martin Corporation. In addition, we thank Dr. Luke Uribarri and Dr. Edward Allen of Lockheed for essential technical oversight. The authors also thank Dr. Kentaro Hara, Dr. Erin Farbar, and Dr. J. P. Sheehan from the University of Michigan for several useful discussions. This research was supported in part through computational resources and services provided by Advanced Research Computing at the University of Michigan, Ann Arbor.

References

[1]Fay, J. A. and Riddell, F. R., "Theory of Stagnation Point Heat Transfer in Dissociated Air," *Journal of the Aeronautics Sciences*, Vol. 25, No. 2, 1958, pp. 73-85.

[2]Voland, R. T., Huebner, L. D., and McClinton, C. R.,"X-43A Hypersonic Vehicle Technology Development," *Acta Astronautica*, Vol. 57, 2005, pp. 614-622.

[3]Glass, D. E., "Physical Challenges and Limitations Confronting the Use of UHTCs on Hypersonic Vehicles," *AIAA Paper 2011-2304*, April 2011.

[4]Uribarri, L. A. and Allen, E. H., "Electron Transpiration Cooling for Hot Aerospace Surfaces," *AIAA Paper 2015-3674*, July 2015.

[5]Alkandry, H., Hanquist, K. M., and Boyd, I. D.,"Conceptual Analysis of Electron Transpiration Cooling for the Leading Edges of Hypersonic Vehicles," *AIAA Paper 2014-2674*, June 2014.

[6]Hanquist, K. M. and Boyd, I. D., "Comparisons of Computations with Experiments for Electron Transpiration Cooling at High Enthalpies," *AIAA Paper 2015-2351*, 2015.

[7]Martin, A., Scalabrin, L. C., and Boyd, I. D., "High Performance Modeling of Atmospheric Re-Entry Vehicles," *Journal of Physics: Conference Series*, Vol. 341, No. 1, 2012, Article 012002.

[8]Wilke, C. R., "A Viscosity Equation for Gas Mixtures," *Journal of Chemical Physics*, Vol. 18, No. 4, 1950, pp. 517-519.

[9]Vincenti, W. G. and Kruger, C. H., *Introduction to Physical Gas Dynamics*, Krieger Publishing Company, New York, 2002.

[10]Blottner, F. G., Johnson, M., and Ellis, M.,"Chemically Reacting Viscous Flow Program for Multi-Component Gas Mixtures," Report No. SC-RR-70-754, Sandia Laboratories, Albuquerque, New Mexico, 1971.

[11]Park, C, *Nonequilibrium Hypersonic Aerothermodynamics*, John Wiley & Sons, New York, 1990.

[12]MacCormack, R. W. and Candler, G. V.,"The Solution of the Navier-Stokes Equations using Gauss-Seidel Line Relaxation," *Computers and Fluids*, Vol. 17, No. 1, 1989, pp. 135-150.

[13]Karypis, G. and Kumar, V., *METIS: A Software Package for Partitioning Unstructured Graphs, Partitioning Meshes, and Computing Fill-Reducing Ordering of Sparse Matrices*, University of Minnesota, Minneapolis, MN, 1998.

[14]Richardson, O. W., *The Emission of Electricity from Hot Bodies*, Longmans, Green and Co., London, 1921.

[15]Haynes, W. M., *CRC Handbook of Chemistry and Physics*, CRC Press, Boca Raton, FL, 2013.

[16]Scott, C. D., "Wall Catalytic Recombination and Boundary Conditions in Nonequilibrium Hypersonic Flows - with Applications," *Advances in Hypersonics - Modeling Hypersonic Flows*, Vol. 2, 1992, pp. 176-250.

[17]Razier, Y. P., *Gas Discharge Physics*, Springer-Verlag, Berlin, 1991.

[18]Sutton, K., and Gnoffo, P. A.,"Multi-component diffusion with application to computational aerothermodynamics," *AIAA Paper 1998-2575*, 1998.

[19]Baeva, M., Kozakov, R., Gorchakov, S., and Uhrlandt, D., "Two-temperature chemically non-equilibrium modeling of transferred arcs," *Plasma Sources Science and Technology*, Vol. 21, 2012, pp. 1-13.

[20]Eiceman, G. A. and Karpas, Z.,"Mobility of Ions in the Gas Phase," *Ion Mobility Spectrometry*, 2nd ed., Taylor and Francis, 2005, pp. 39-68.

[21]Wright, M. J., Hwang, H. H., and Schwenke, D. W., "Recommended Collision Integrals for Transport Property Computations Part 2: Mars and Venus Entries," *AIAA Journal*, Vol. 45, No. 1, 2007, pp. 281-288.

[22]Karpas, Z., Berant, Z., and Shahal, O., "Effect of Temperature on the Mobility of Ions," *Journal of American Chemical Society*, Vol. 111, No. 16, 1989, pp. 6015-6018.

[23]Fridman, A., and Kennedy, L. A., *Plasma Physics and Engineering*, Taylor & Francis, New York, 2004.

[24]Sheridan, T. E., and Goree, "Collisional plasma sheath model," *Physics of Fluids B: Plasma Physics*, Vol. 3, 1991, pp. 2796-2804.

[25]Lieberman, M. A. and Lichtenberg, A. J., *Principles of Plasma Discharges and Materials Processing*, John Wiley & Sons, New York, 1994.

[26]Benilov, M. S. and Marotta, A., "A Model of the Cathode Region of Atmospheric Pressure Arcs," *Journal of Physics D: Applied Phyiscs*, Vol. 28, No. 9, 1995, pp. 1869-1882.

[27]Hobbs, G. D., and Wesson, J. A., "Heat Flow Through a Langmuir Sheath in the Presence of Electron Emission," *Plasma Physics*, Vol. 9, No. 1, 1967, pp. 85-87.

[28]Ye, M. Y. and Takamura, S., "Effect of Space-Charge Limited Emission on Measurements of Plasma Potential Using Emissive Probes," *Physics of Plasmas*, Vol. 7, No. 8, 2000, pp. 3457-3463.

[29]Hara, K., "Development of Grid-Based Direct Kinetic Method and Hybrid Kinetic Continuum Modeling of Hall Thruster Discharge Plasma," Ph. D. Dissertation, Department of Aerospace Engineering, University of Michigan, Ann Arbor, MI, 2015.